HAL
open science

Structural, magnetic, and insulator-to-metal transitions under pressure in the GaV4S8 Mott insulator: A rich phase diagram up to 14.7 GPa

J. Mokdad, G. Knebel, C. Marin, J.-P. Brison, V. Ta Phuoc, Rodolphe Sopracase, Claire Colin, D. Braithwaite

To cite this version:

J. Mokdad, G. Knebel, C. Marin, J.-P. Brison, V. Ta Phuoc, et al.. Structural, magnetic, and insulator-to-metal transitions under pressure in the GaV4S8 Mott insulator: A rich phase diagram up to 14.7 GPa. Physical Review B, 2019, 100 (24), pp.245101. 10.1103/PhysRevB.100.245101 . cea-02496662

HAL Id: cea-02496662

https://cea.hal.science/cea-02496662

Submitted on 3 Mar 2020

HAL is a multi-disciplinary open access archive for the deposit and dissemination of scientific research documents, whether they are published or not. The documents may come from teaching and research institutions in France or abroad, or from public or private research centers.

L'archive ouverte pluridisciplinaire **HAL**, est destinée au dépôt et à la diffusion de documents scientifiques de niveau recherche, publiés ou non, émanant des établissements d'enseignement et de recherche français ou étrangers, des laboratoires publics ou privés.

Structural, magnetic, and insulator-to-metal transitions under pressure in the GaV_4S_8 Mott insulator: A rich phase diagram up to 14.7 GPa

J. Mokdad,[1,*] G. Knebel,[1] C. Marin,[1] J.-P. Brison,[1] V. Ta Phuoc,[2] R. Sopracase,[2] C. Colin,[3] and D. Braithwaite[1]
[1]*Université Grenoble Alpes, CEA, IRIG-Pheliqs, 38000 Grenoble, France*
[2]*GREMAN-UMR 7347 CNRS - Université de Tours. Parc de Grandmont, 37200 Tours, France*
[3]*Université Grenoble Alpes, CNRS, Institut Néel, 38000 Grenoble, France*

(Received 17 September 2019; revised manuscript received 29 October 2019; published 2 December 2019)

In addition to its promising potential for applications, GaV_4S_8 shows very interesting physical properties with temperature and magnetic field. These properties can be tuned by applying hydrostatic pressure in order to reveal and understand the physics of these materials. Not only pressure induces an insulator-to-metal transition in GaV_4S_8 but it also has an interesting effect on the structural and magnetic transitions. Using a combination of AC calorimetry, capacitance, and resistivity measurements under pressure, we determine the evolution of the structural and magnetic transitions with pressure and thus establish the T-P phase diagram of GaV_4S_8. To detect the insulator-to-metal transition (IMT), we use optical conductivity and DC resistivity measurements and we follow the evolution of the Mott gap under pressure. The structural transition temperature increases with pressure and a second transition appears above 6 GPa indicating a possible new phase with a very small gap. Pressure has a surprisingly very weak effect on the ferromagnetic transition that persists even very close to the IMT that occurs at around 14 GPa, implying that the metallic state may also be magnetic.

DOI: 10.1103/PhysRevB.100.245101

I. INTRODUCTION

GaV_4S_8 is a lacunar spinel Mott insulator that has gained a lot of attention in the past few years due to its potential applications in Mott memories and neuromorphic computing, in addition to its interesting physical properties and rich phase diagram at low temperatures and magnetic fields [1]. The lacunar spinels are a special kind of Mott insulators due to the fact that the electrons are highly localized within metal clusters (see Fig. 1) and not localized on atomic sites as in a usual Mott insulator. It is the long intercluster distance of about 4 Å [2] that keeps the electrons from circulating and thus makes the material insulating. Many studies exist on GaV_4S_8 at ambient pressure [2–4] showing a ferroelectric Jahn-Teller symmetry-lowering structural transition at 43.3 K from cubic $F\bar{4}3m$ to rhombohedral $R3m$ and a transition to a ferromagnetic state at 12.7 K, which contains skyrmionic and cycloidal phases at low temperature and low magnetic field.

Therefore, the application of hydrostatic pressure is a very pertinent tool in the lacunar spinel family since it decreases the intercluster distance and hence increases the transfer interaction while maintaining the same lattice structure [5]. In other words, by forcing the clusters closer together, the material could become conducting by hopping of the electrons between the clusters. By this procedure, pressure can induce Mott insulator-to-metal transitions. Several electrical transport studies exist on these materials showing a transition to a metallic phase and even the emergence of superconductivity in some members of the family [6], although this study was not performed on GaV_4S_8. Moreover, these resistivity studies were not able to explore inside the insulating state, so the high pressure/low-temperature phase diagrams of these systems are unknown. We initiated this study, to reveal the insulator to metal transition in GaV_4S_8 and also to establish the effect of pressure on the rich low-temperature phase diagram. To achieve this we combined specific heat, capacitance, and resistivity measurements, under pressure up to 14.7 GPa in a diamond anvil cell with *in situ* pressure tuning. We have determined the evolution under pressure of the temperature of the structural and magnetic transitions and thus established the detailed T-P phase diagram. We also follow the evolution of the gap energy with pressure and reveal the insulator-to-metal transition, both with transport and optical conductivity experiments. We find that the structural transition temperature T_S increases with pressure and we detect a second anomaly at high pressure. We find two different insulating or semiconducting regimes at temperatures above and below the structural transition, and above a pressure of about 10 GPa the low-temperature state is a small gap semiconductor. The system becomes fully metallic at around 14 GPa. The magnetic transition temperature stays relatively stable with pressure and magnetism persists at least up to 12 GPa close to the insulator-to-metal transition (IMT) at around 14 GPa. No sign of superconductivity was observed.

II. EXPERIMENTAL DETAILS

Single crystals of GaV_4S_8 were grown using vapor- phase transport method in a multizone tube furnace with iodine as a transport agent. The crystals were characterized and oriented by x-ray Laue diffraction. The [111] crystallographic

*Julia.MOKDAD@cea.fr

 ©2019 American Physical Society

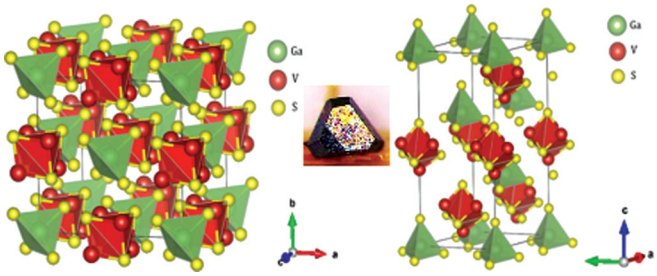

FIG. 1. The cubic lattice structure of the lacunar spinel GaV_4S_8 at 300 K (left) with a $F\bar{4}3m$ symmetry and a lattice parameter of $a = 9.661$ Å [7]. The tetrahedral $(GaS_4)^{5-}$ cluster and the cubane $(V_4S_4)^{5+}$ clusters are presented in green and red respectively. At $T_S = 43.3$ K, a Jahn-Teller transition causes an elongation in the V_4 and GaS_4 tetrahedra which reduces the symmetry to rhomboedric $R3m$ (right). The inset of Fig. 1 shows a crystal obtained by the vapor-phase transport growth with a large triangular face perpendicular to the [111] crystallographic direction.

direction was determined by Laue diffraction as perpendicular to the large triangular surface of the crystal (see Fig. 1). Specific heat and magnetization measurements were made in commercial devices (Quantum Design PPMS and MPMS). The ambient pressure phase diagram versus temperature and magnetic field was determined from the magnetization measurements as well as pyrocurrent measurements, performed using a Keithley Electrometer as a function of temperature between 2 and 100 K and fields between 0 and 200 mT. These measurements were carried out on relatively large single crystals.

Measurements under hydrostatic pressure (except for optical conductivity) were performed in a diamond anvil cell (DAC) with liquid argon as a pressure transmitting medium. For these experiments, samples were polished to a thickness of about 30–40 μm perpendicular to [111], then cut to fit into the pressure chamber. All the samples used for measurements under pressure have typical dimensions of around $200 \times 250 \times 40\,\mu m^3$. Pressure was changed using a recently developed *in situ* pressure tuning system that relies on a mechanical screw device. In contrast to a previous system using helium bellows, this system can be used over the whole temperature range 2–300 K. The pressure was determined *in situ* by the ruby fluorescence technique. The low-temperature measurements were carried out in a helium flow cryostat allowing to cool the sample down to 2.3 K and a magnetic field up to 9 T could be applied.

AC calorimetry measurements under pressure were done in the DAC on a $150 \times 250 \times 30\,\mu m^3$ GaV_4S_8 sample following the procedure described by Demuer *et al.* [8]. The sample was heated optically with a laser chopped at a frequency of 1 kHz. An AuFe/Au thermocouple was attached to the sample. The amplitude and phase shift of the temperature oscillations were measured with lock-in detection. For dielectric measurements, a thin layer of gold was evaporated onto both sides of the sample to which wires were attached. We used an Andeen-Hagerling AH 2550A 1kHz capacitance bridge that allows us to measure the capacitance C (pF) proportional to the dielectric constant of the sample and the loss (nS) that is inversely proportional to the resistance. The bridge can measure correctly when the resistance of the sample is of the order of 10 kΩ or higher. For measurements at high temperature or high pressure when the sample was less resistive than this, we performed 2 lead DC resistivity measurements using a current source and nanovoltmeter. The total resistance of the current leads and contacts was about 60 Ω and varied by less than 10% over the whole temperature range. Thermal hysteresis between warming and cooling was less than 1.5% coming mainly from thermal lag between the sample and the thermometer. No significant intrinsic hysteresis or memory effects were observed.

Room-temperature pressure-dependent optical conductivity spectra have been deduced from nearly normal incidence sample-diamond reflectivity $R_{sd}(\omega)$ between 550 and 12 000 cm^{-1} wave numbers (8000 cm^{-1} = 1 eV) on a $100 \times 100\,\mu m^2$ single crystal from 0 to 17.5 GPa using a BETSA membrane diamond anvil cell. The sample was loaded inside a gasket hole together with KBr as a hydrostatic medium. The gasket was used as a reference mirror. $R_{sd}(\omega)$ was measured by using a homemade high-vacuum microscope including an X15 Schwarzchild objective connected to a BRUKER IFS 66v/S Fourier Transform Spectrometer with a Mercury-Cadmium-Telluride detector, Glowbar, and tungsten light sources. Pressure was measured with the standard ruby fluorescence technique. In order to obtain the optical conductivity from the $R_{sd}(\omega)$, we used a variational dielectric function method [9].

III. RESULTS

A. Phase diagram of GaV_4S_8 at ambient pressure

At $T_m = 12.7$ K, GaV_4S_8 undergoes a magnetic transition that was first thought to be an ordinary ferromagnetic transition [2,10]. Later it was found that in fact, at 12.7 K, the material enters a cycloidal phase before becoming a normal ferromagnet at lower temperatures. The phase diagram becomes even richer when applying magnetic field in the ⟨111⟩ direction, with different magnetic phases emerging up to 110 mT [1–3].

Figure 2 presents the phase diagram obtained on our single crystals of GaV_4S_8 at ambient pressure based on magnetization, pyrocurrent, and specific heat measurements with a magnetic field applied along the ⟨111⟩ direction. The nature of the different phases has been identified by comparison to other published phase diagrams [1–3]. The field derivative of the magnetization, with $B//\langle 111\rangle$, and the pyrocurrent both show sharp peaks corresponding to the transitions between the different magnetic phases (see inset of Fig. 2). Our results are in quite good agreement with the previous studies. With pyrocurrent and magnetization measurements we detect two magnetic states corresponding to the reported cycloidal and skyrmionic phases that persist up to 20 and 70 mT, respectively, at 12.5 K with the magnetic field parallel to the [111] direction. However, the pyrocurrent measurement shows a clear anomaly at 13 mT at 5 K (see inset Fig. 2) that persists down to 4 K and only disappears completely at 2 K, implying that the cycloidal phase at zero field persists to temperatures down to 3 K before becoming ferromagnetic.

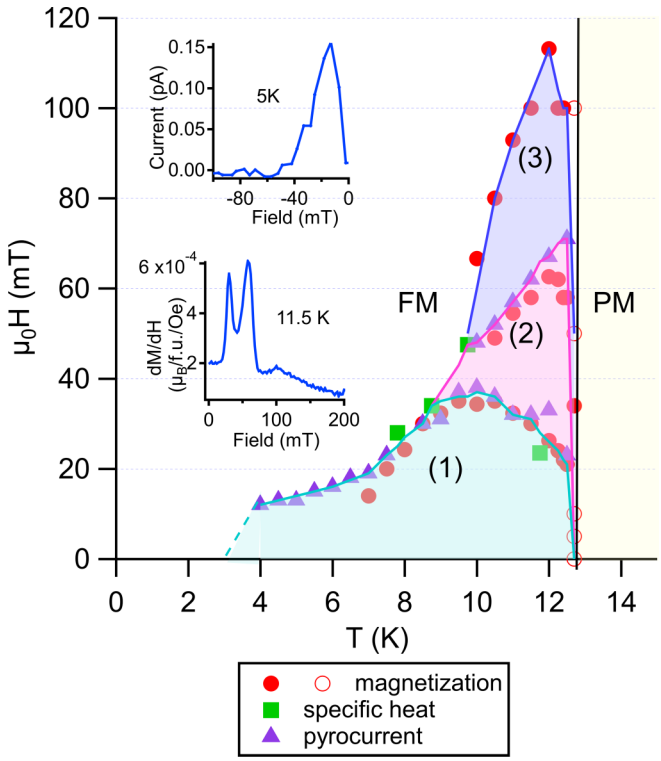

FIG. 2. Phase diagram of GaV_4S_8 at ambient pressure. The phase boundaries as determined by magnetization, specific heat, and pyrocurrent measurements are indicated by circles, squares, and triangles respectively. Three magnetic phases indicated as (1), (2) and (3) correspond to one cycloidal and two skyrmionic phases, respectively, by comparison with the phase diagram published by Kezsmarki *et al.* [2]. The first inset shows the anomaly at 13 mT in the pyrocurrent (pA) at 5 K. The curve has been shifted by 13 mT so that the curves of the positive and negative field sweep are symmetric at zero field. The second inset presents the field-derivative of magnetization versus field at 11.5 K: three anomalies appear at 30, 58, and 100 mT indicating the transitions between the three magnetic phases.

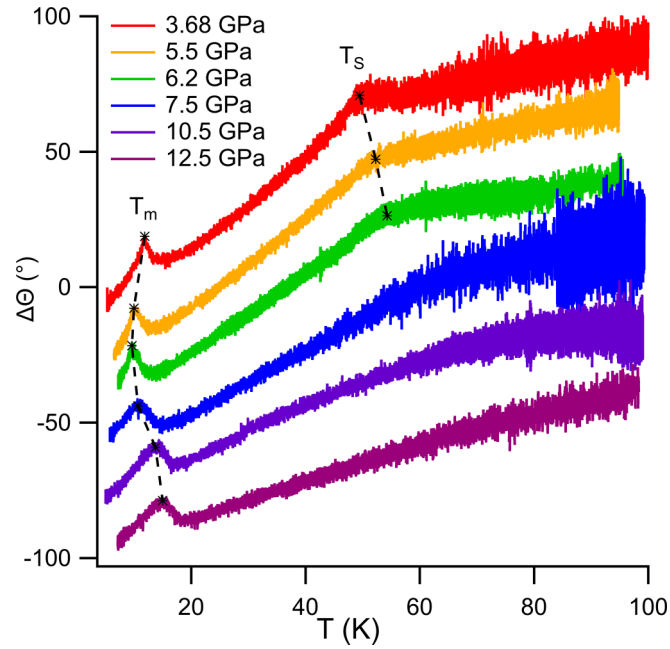

FIG. 3. Temperature dependence of the phase $\Delta\Theta$ in AC calorimetry measurements in GaV_4S_8 for different pressures. The curves are shifted vertically for clarity. The magnetic and structural transitions are marked by asterisks and the dashed lines are guide to the eye to show the variation of T_m and T_S with pressure. For pressures above 7.5 GPa, the structural transition becomes nearly invisible.

B. Measurements under pressure

1. AC Calorimetry measurements

In the AC calorimetry measurements (Fig. 3), we found that the phase shift $\Delta\Theta$ of the signal is more sensitive to the phase transitions than the temperature oscillation amplitude T_{ac}. The magnetic transition appears as a well-defined peak in the phase of the signal, and the aspect of the transition remains almost unchanged over the whole pressure range explored here, up to 12.5 GPa. The magnetic transition temperature T_m decreases slightly with pressure from 12.7 K at ambient pressure, passes by a minimum of $T_m = 9.6$ K at 6 GPa then increases again to reach $T_m = 15$ K at 12.5 GPa. So surprisingly pressure has a rather weak effect on the magnetic transition in GaV_4S_8, over a pressure range of 12.5 GPa. (See phase diagram in Fig. 9).

The structural transition is more difficult to track under pressure with AC calorimetry. Although in the ambient pressure specific heat measurement it appears as a large anomaly, being a first-order transition, the anomaly can be hugely attenuated in the AC measurement. At low pressure it starts out as a small peak that gets smeared out when pressure increases and becomes nearly invisible above 6.2 GPa.

As an overall behavior, the temperature of the structural transition T_S begins at 43.3 K at ambient pressure and increases up to 55 K at 7 GPa.

Since the magnetic transition stays relatively stable under pressure and the structural transition anomaly is rather weak, AC calorimetry does not give any indication of the expected IMT. Therefore we performed dielectric measurements using a capacitance bridge, which allows measuring the dielectric constant and the resistivity simultaneously.

2. Dielectric measurements

Figure 4 presents the temperature dependence of the capacitance (pF) and loss (nS) measured simultaneously by the capacitance bridge for different pressures. At 1.45 GPa the capacitance bridge only measures below 120 K when the resistance of the sample is greater than 6.7 kΩ. In contrast to the AC calorimetry measurement, at pressures up to 6 GPa, the structural transition shows up here as a huge anomaly in both the capacitance and the loss. We take the maximum of the peak in capacitance and loss curves as a criterion to determine the temperature of the structural transition (see Fig. 4).

The transition is clearly visible in both the capacitance and the loss up to 6 GPa and the transition temperature T_S initially increases with pressure. At higher pressure the anomaly in the loss disappears. In the capacitance measurements above 6.9 GPa, the peak that seems to correspond to T_S is transformed into a wide bump that shifts to lower temperatures and another marked peak that we will mark as T_X appears at higher

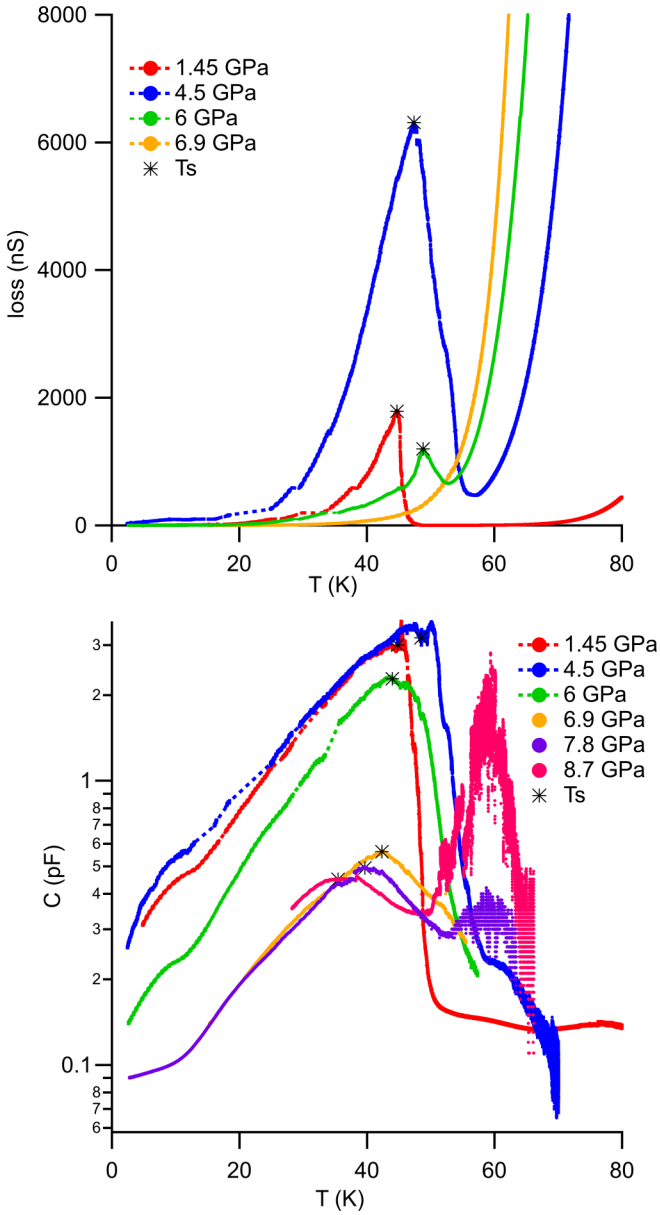

FIG. 4. (Top graph) Loss versus temperature under pressure. The loss shows a peak for the structural transition T_S. It is marked by asterisks on the curves. T_S increases with pressure and becomes invisible at 6.9 GPa. (Bottom graph) Capacitance versus temperature under pressure showing one peak for the structural transition T_S for pressures below 7.8 GPa. Above this pressure, T_S gets smeared out and another peak T_x appears at higher temperatures. T_S has been marked by asterisks on the curves.

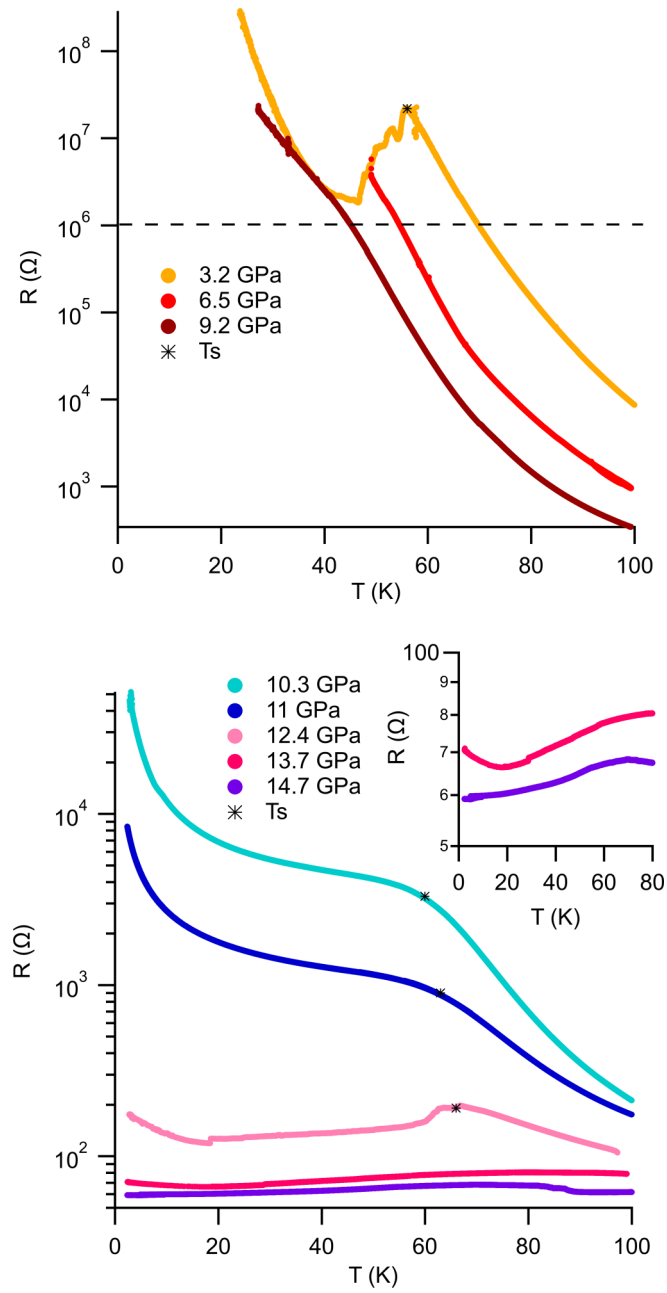

FIG. 5. Temperature dependence of the DC resistance in GaV_4S_8 for different pressures. The structural transition is marked by an asterisk. T_S has been determined from the intersection of the two lines drawn tangent to the resistance curves $R(T)$ around the anomaly. The inset shows the resistance vs temperature for 13.7 and 14.7 GPa showing an insulator-to-metal transition. A dashed line at 1 MΩ indicates the value above which the measured resistance becomes unreliable.

temperature. The capacitance bridge stops measuring at pressures above 9.2 GPa when the loss becomes too high to measure (electrical resistance too low) and the capacitance becomes too low.

3. DC Resistivity measurements

Two-lead DC resistivity measurements were performed in the pressure/temperature ranges where the sample resistance was too low to measure with the capacitance bridge, and to some extent for intermediate resistance values where both types of measurement were carried out. This technique allowed values of resistance up to about 1 MΩ to be measured reliably. Figure 5 shows the temperature dependence of the electrical resistance of the sample in the temperature range below 100 K as a function of pressure for GaV_4S_8. At low pressures, the resistance shows a semiconducting like behavior with the structural transition clearly visible at 3.2 GPa. The transition gets smeared out with increasing pressure which

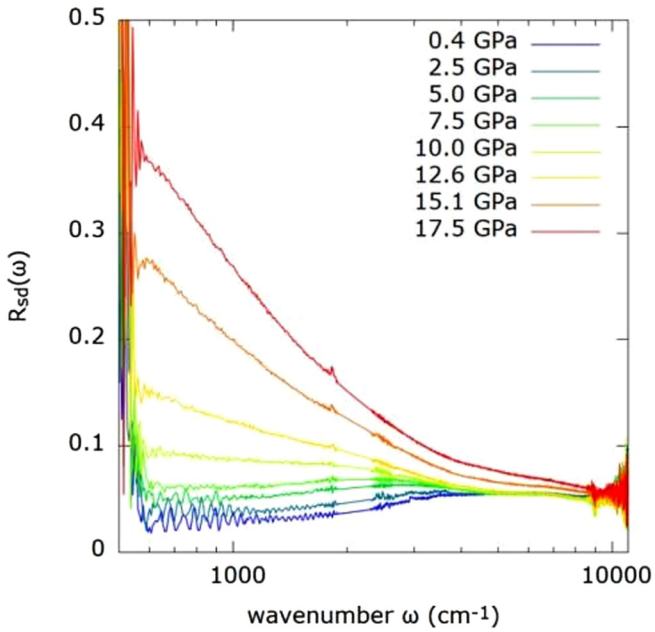

FIG. 6. Pressure dependence of the reflectivity spectra at the sample-diamond interface.

makes it difficult to determine the exact value of T_S up to 9.2 GPa. However above this pressure, as the sample becomes less semiconducting the transition actually becomes more pronounced again.

At 13.7 GPa, the resistance of the sample decreases with decreasing temperature except at very low temperatures where a semiconducting behavior is still found. A metallic-like behavior appears at 14.7 GPa over the whole temperature range.

4. Reflectivity measurements

Pressure-dependent reflectivity spectra at the sample-diamond interface $R_{\mathrm{sd}}(\omega)$ are shown in Fig. 6. Strong two-photon diamond absorption prevents the measurement of R_{sd} between 1750 and 2700 cm^{-1}.

On increasing the pressure from 0 to 17.5 GPa, the reflectivity is progressively enhanced at low frequency. Up to 5 GPa, Fabry-Perot interferences can be observed below 2000 cm^{-1} suggesting that the sample behaves like a transparent layer in this frequency range, confirming its insulating nature.

As pressure increases, the fringes disappear, meaning a decrease of the skin depth and the existence of an electronic background at low frequency.

Those results are consistent with an insulator-to-metal transition under pressure. Quantitative information will be extracted from the optical conductivity spectra deduced from R_{sd} (see next section).

C. IMT in GaV_4S_8 under pressure

1. Transport measurements

Another way to determine the insulator-to-metal transition IMT is to follow the variation of the gap energy with pressure. The exponential increase of resistivity to lower temperatures indicates thermal activation of carriers. Therefore, we can

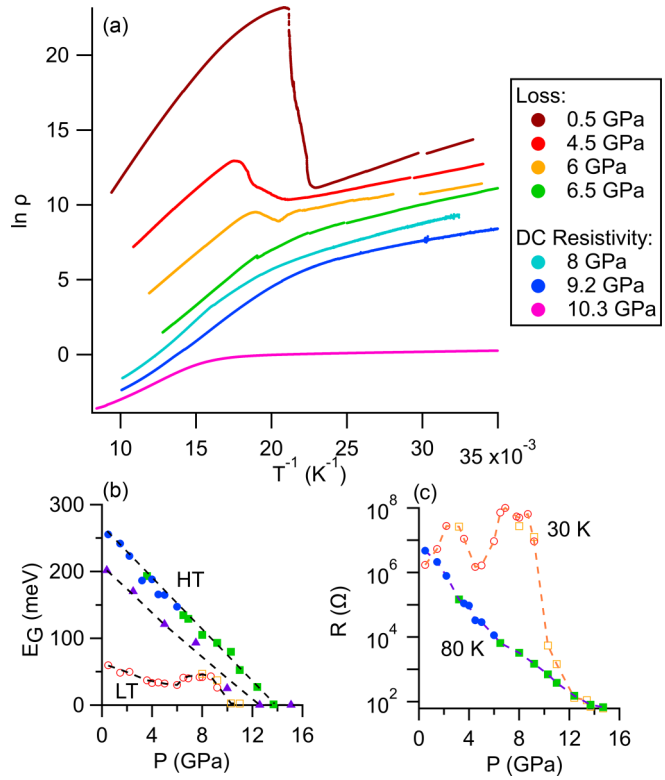

FIG. 7. (a) ln ρ versus T^{-1} showing a linear behavior at high and low temperatures up to 6.5 GPa. The curves are shifted vertically for clarity. (b) Pressure dependence of the gap energy E_G above and below the structural transition (closed and open symbols, respectively) computed from loss, DC resistivity measurements and optical conductivity indicated by circles, squares, and triangles, respectively. The pressure dependence of the optical gap is obtained at room temperature by a standard extrapolation technique. (c) Pressure dependence of the resistance at 80 and 30 K (closed and open symbols, respectively) computed from loss and DC resistivity measurements indicated by circles and squares, respectively.

extract the gap energy from an Arrhenius law:

$$\sigma = \sigma_0\, e^{-\frac{E_G}{2k_B T}}.$$

Figure 7(a) shows the Arrhenius plots for different pressures. At high temperatures above T_S, the thermal activation law is valid and ln $\rho(T^{-1})$ is linear over a wide temperature range up to 8 GPa. Above this pressure the behavior becomes less linear therefore the estimation of the gap energy has been done on a smaller temperature range. Below the structural transition (25 K $< T <$ 45 K), an activation law is still valid with a much smaller gap.

Figure 7(b) shows the pressure dependence of the gap above and below the structural transition. The gap energy determined above the structural transition from resistivity measurements decreases linearly with pressure and by extrapolation a pressure of 14 GPa is found for the IMT in good agreement with the global behavior over the whole temperature range found in the DC resistivity. Studying the pressure dependence of the optical gap at 300 K (see below), one can observe its linearity, similarly to the gap obtained from the Arrhenius law around 100 K. The pressure of the

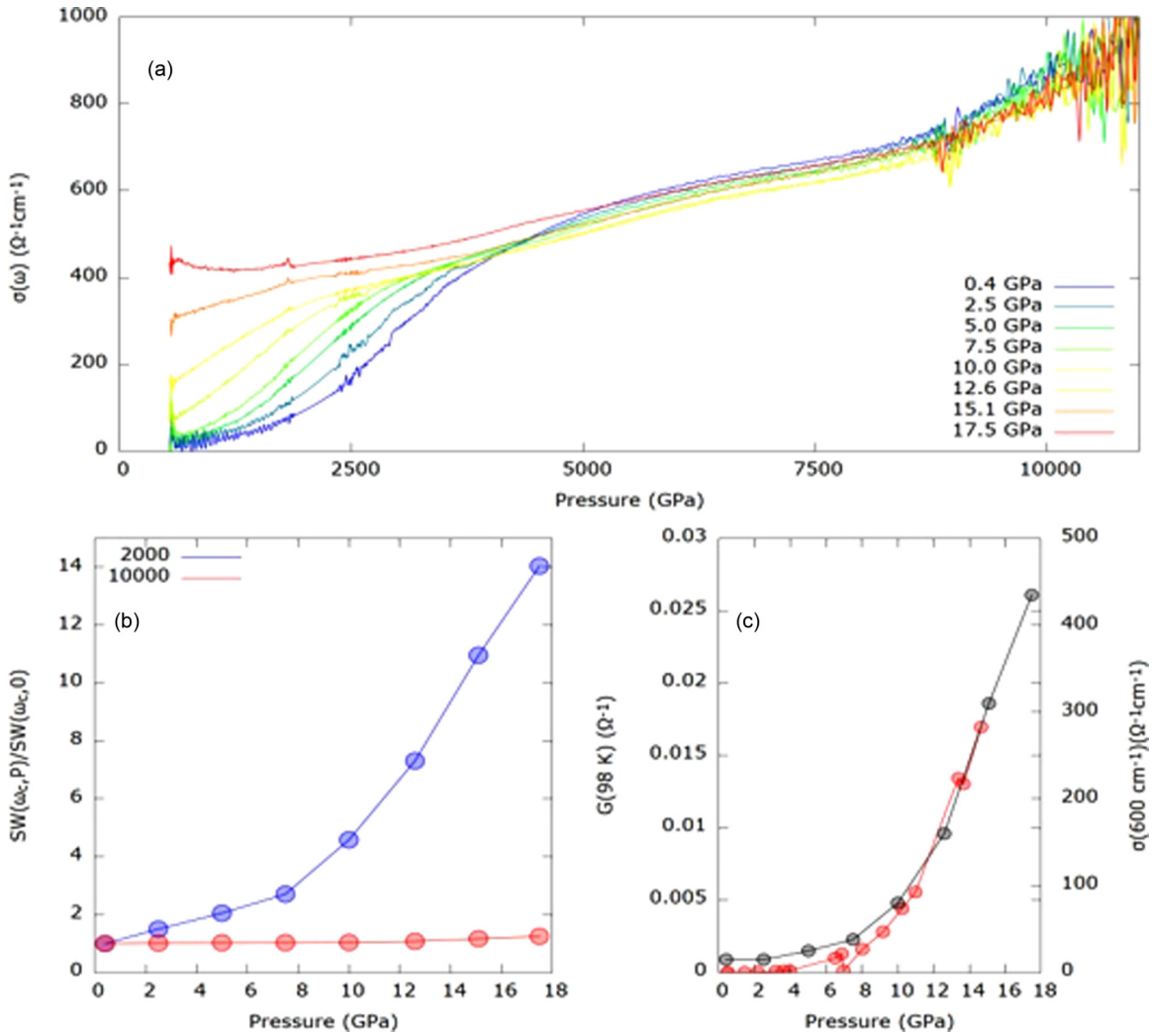

FIG. 8. (a) Pressure dependence of the optical conductivity at room temperature. (b) Pressure dependence of the normalized SW on the whole spectrum (red) and at low energy (blue). (c) Pressure dependence of the lowest measured optical conductivity (gray), pressure dependence of the conductance (red) (obtained from the transport measurements).

IMT obtained by the former technique is 2–3 GPa smaller than the latter.

Below the structural transition we find a semiconducting behavior with a gap of 60 meV, in agreement with low temperature optical conductivity [11]. Up to 6 GPa this gap decreases with pressure almost linearly. Above this pressure, E_G increases to reach a maximum at 8 GPa then decreases again to a very small value, reaching 2.3 meV at 11 GPa.

Figure 7(c) shows a smooth decrease of the resistance at 80 K up to 14.7 GPa. On the other hand, at 30 K, the resistance is relatively stable up to 9.2 GPa then suddenly decreases by several orders of magnitude (see also Fig. 5) to reach 60 Ω at 14.7 GPa, which represents mostly the resistance of the coaxial wires, indicating also the IMT.

2. *Optical conductivity*

The pressure-dependent optical conductivities $\sigma(\omega)$ deduced from the R_{sd} at 300 K are shown in Fig. 8(a). The ambient pressure $\sigma(\omega)$ consists of a broad midinfrared band centered around 0.6 eV (5000 cm^{-1}) and the tail of higher energy excitations consistently with Reschke *et al.* [11]. An optical gap of 200 meV (1600 cm^{-1}) can be extracted by the standard extrapolation procedure, consistently with the 250 meV obtained from transport measurements [see Fig. 7(b)]. Note that the gap is substantially larger than for isostructural $GaTa_4Se_8$ [12] (120 meV).

With increasing pressure, the optical gap progressively closes up to 10 GPa. Between 10 and 12.6 GPa, the system undergoes an IMT and the extrapolation of $\sigma(\omega)$ at low-frequency σ_{opt} increases with pressure. At the highest pressure, the onset of a narrow Drude peak, characteristic of a metallic behavior is observed.

Figure 8(c) depicts the pressure evolution of the lowest measured $\sigma(\omega)[\sigma(600\,\mathrm{cm}^{-1})]$ at 300 K in the Insulating Paramagnetic paraelectric phase and the conductance measured by transport at 98 K in the same thermodynamic phase. Both curves are very similar, they both show a steep increase at some pressure, which is the signature of the IMT.

The spectral weight (SW) defined as

$$\mathrm{SW}_{\Omega_0}^{\Omega}(P) = \int_{\Omega_0}^{\Omega} \sigma(\omega, P) d\omega,$$

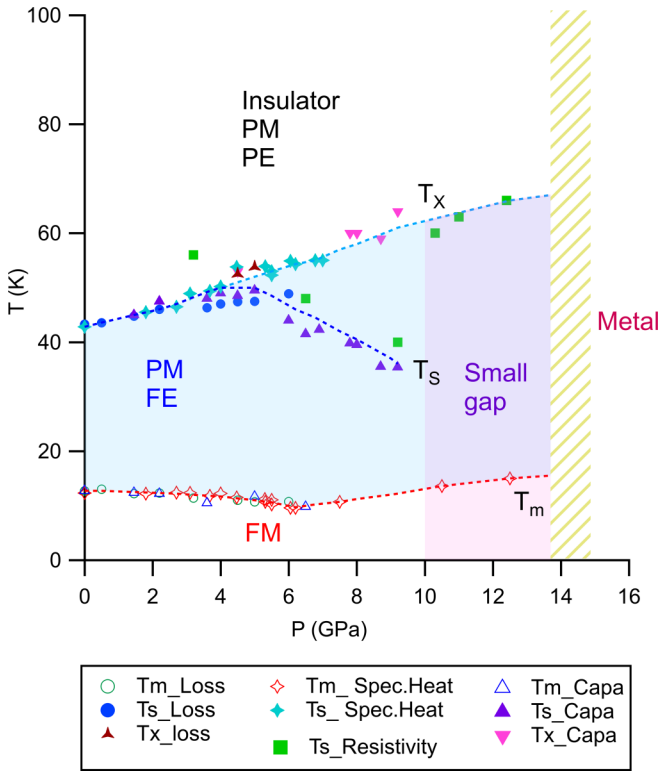

FIG. 9. T-P phase diagram of GaV_4S_8 determined by specific heat, capacitance, and resistivity measurements under pressure up to 14.7 GPa. Dotted lines are guides for the eye.

is proportional to the charge carrier density involved in the $[\Omega_0, \Omega]$ frequency range.

In the insulating phase, when P increases, some spectral weight is transferred from high to low energy, filling the gap region and evidencing an isosbestic point around 0.5 eV ($4000\,\mathrm{cm}^{-1}$) in the optical conductivity spectra. From 12.6 to 17.5 GPa, there is no more spectral weight transfer as the whole spectrum increases with pressure. To be more quantitative, Fig. 8(b) shows the total measured SW (up to $10\,000\,\mathrm{cm}^{-1}$) and the low frequency SW (up to $2000\,\mathrm{cm}^{-1}$). Total SW increases by ~20% from lowest to highest pressure meaning an almost SW conservation below 1.25 eV. On the contrary, low frequency SW drastically increases with pressure. Such a SW transfer over a large energy scale under pressure is a usual fingerprint of strongly correlated systems [12].

D. Phase diagram of GaV_4S_8 under pressure

Figure 9 shows the phase diagram of GaV_4S_8 under pressure up to 14.7 GPa determined from ac calorimetry, capacitance and resistivity measurements under pressure.

Considering the overall behavior of the transitions, we can see that T_S increases when applying pressure from 43.3 K at ambient pressure to about 55 K at 6 GPa. At higher pressures two anomalies are seen, one (labeled T_X as a second peak in the capacitance and a kink in the DC resistance measurements) continues to shift to higher temperatures, and a second one, which seems to be the continuation of T_S in the capacitance measurements that moves to lower temperatures. The shape of the anomaly in the ac calorimetry is stable over the whole pressure range, and the magnetic transition temperature slightly changes little with pressure, although a minimum is seen around 6 GPa.

IV. DISCUSSION

In this T-P phase diagram, one could clearly note three different insulating/semiconducting regimes.

(1) At ambient pressure, the material is a Mott insulator in the cubic high-temperature phase with a Mott gap of 260 meV and becomes semiconducting below the structural transition with a 60 meV gap. The gap below the structural transition becomes smaller when the pressure increases up to 6 GPa. It is interesting to mention that some theoretical studies [13,14] predict that the structural distortion might open a gap at the Fermi level even without strong electronic correlations, whereas we find actually a smaller gap in the low temperature phase.

(2) Between 6 and 10 GPa, an additional phase transition appears. Further studies are necessary to determine its nature. We have noticed that in this pressure range the initial structural transition T_S becomes less marked. This is seen in AC calorimetry measurements where T_S becomes invisible, the peak in resistivity disappears, and the peak in the capacitance gets smeared out. The gap energy below the structural transition becomes larger above 6 GPa and the conduction regime starts to deviate from the thermal activation law.

(3) The Mott gap determined from the high-temperature resistivity decreases linearly with pressure, reaching zero at around 14.2 GPa±0.4 GPa, and at this pressure GaV_4S_8 becomes fully metallic. However above 10 GPa the low temperature gap becomes very small and the absolute value of the resistance decreases by several orders of magnitude at low temperatures (see Fig. 7). So in quite a large P-T range the system is a rather small gap semiconductor. These results are confirmed by optical conductivity at 300 K where a closing of the gap at around 12.5 GPa is found. Note that other members of the lacunar spinel family undergo this IMT at close pressures: 15 GPa for $GaTa_4Se_8$ and 19 GPa for $GaNb_4Se_8$ [6]. In GaV_4S_8 the anomaly due to the magnetic transition is clearly visible in AC calorimetry measurements up to 12.5 GPa, although we cannot rule out a change in the type of magnetic order. So the small gap phase is almost certainly magnetic and possibly the high pressure metallic phase may be too, so at low temperature GaV_4S_8 may switch from a ferromagnetic insulator to a ferromagnetic metal. This has been seen in other Mott insulators like Ca_2RuO_4 [15] where the IMT happens with the material staying magnetic.

Even in the metallic state we found no superconductivity in GaV_4S_8, whereas it has been seen in other members of the spinel family like $GaTa_4Se_8$ and $GaNb_4Se_8$ even slightly before the IMT [6]. Nevertheless these compounds do not exhibit structural transitions and remain in the cubic phase over a broad temperature range [6]. They also show very weak magnetism and do not exhibit magnetic ordering down to 1.6 K [6,13], contrary to GaV_4S_8, which is ferromagnetic below T_m.

V. CONCLUSION

GaV_4S_8 presents a rich T-P phase diagram with a structural transition increasing to higher temperatures with

pressure and the emergence of a second transition at high pressure. To our knowledge, this would be the first phase diagram showing the evolution of the structural and magnetic transitions under pressure in a lacunar spinel. Supplementary measurements are required to follow the nature of the structural changes in GaV_4S_8 under pressure and determining the magnetic properties of the different phases and the nature of the new phase limited by T_X. We observed a pressure-induced insulator-to-metal transition between 10 and 12.6 GPa at 300 K that shifts to 14 GPa at low temperatures. Interestingly, the Mott gap in the cubic high temperature phase decreases linearly with pressure and closes at the IMT. On the other hand, a smaller gap at low temperatures closes at a lower pressure. The material stays ferromagnetic at least up to the IMT and further measurements are needed to determine if it stays ferromagnetic in the metallic phase as well.

ACKNOWLEDGMENTS

D.B. acknowledges the contributions of A. Huxley and P. Attfield to implement capacitive measurements in the diamond anvil cell. J.M. acknowledges financial support from the CEA "Amont-Aval" Ph.D. program.

[1] I. Kézsmárki, S. Bordács, P. Milde, E. Neuber, L. M. Eng, J. S. White, H. M. Rønnow, C. D. Dewhurst, M. Mochizuki, K. Yanai, H. Nakamura, D. Ehlers, V. Tsurkan, and A. Loidl, Néel-type skyrmion lattice with confined orientation in the polar magnetic semiconductor GaV_4S_8, Nat. Mater. **14**, 1116 (2015).

[2] R. Pocha, D. Johrendt, and R. Pöttgen, Electronic and structural instabilities in GaV_4S_8 and $GaMo_4S_8$, Chem. Mater. **12**, 2882 (2000).

[3] E. Ruff, S. Widmann, P. Lunkenheimer, V. Tsurkan, S. Bordács, I. Kézsmárki, and A. Loidl, Multiferroicity and skyrmions carrying electric polarization in GaV_4S_8, Sci. Adv. **1**, e1500916 (2015).

[4] S. Widmann, E. Ruff, A. Günther, H.-A. K. von Nidda, P. Lunkenheimer, V. Tsurkan, S. Bordács, I. Kézsmárki, and A. Loidl, On the multiferroic skyrmion-host GaV_4S_8, Philos. Mag. **97**, 3428 (2017).

[5] M. Imada, A. Fujimori, and Y. Tokura, Metal-insulator transitions, Rev. Mod. Phys. **70**, 1039 (1998).

[6] M. M. Abd-Elmeguid, B. Ni, D. I. Khomskii, R. Pocha, D. Johrendt, X. Wang, and K. Syassen, Transition from Mott Insulator to Superconductor in $GaNb_4Se_8$ and $GaTa_4Se_8$ Under High Pressure, Phys. Rev. Lett. **93**, 126403 (2004).

[7] Y. Sahoo and A. K. Rastogi, Evidence of hopping conduction in the V4-cluster compound GaV_4S_8, J. Phys.: Condens. Matter **5**, 5953 (1993).

[8] A. Demuer, C. Marcenat, J. Thomasson, R. Calemczuk, B. Salce, P. Lejay D. Braithwaite, and J. Flouquet, Calorimetric study of $CeRu_2Ge_2$ under continuously swept hydrostatic pressure up to 8 GPa, J. Low Temp. Phys. **120**, 245 (2000).

[9] A. B. Kuzmenko, Kramers-Kronig constrained variational analysis of optical spectra, Rev. Sci. Instrum. **76**, 083108 (2005).

[10] C. S. Yadav, A. K. Nigam, and A. K. Rastogi, Thermodynamic properties of ferromagnetic Mott-insulator GaV_4S_8, Physica B **403**, 1474 (2008).

[11] S. Reschke, F. Mayr, Z. Wang, P. Lunkenheimer, Weiwu Li, D. Szaller, S. Bordács, I. Kézsmárki, V. Tsurkan, and A. Loidl, Optical conductivity in multiferroic GaV_4S_8 and GeV_4S_8: Phonons and electronic transitions, Phys. Rev. B **96**, 144302 (2017).

[12] V. T. Phuoc, C. Vaju, B. Corraze, R. Sopracase, A. Perucchi, C. Marini, P. Postorino, M. Chligui, S. Lupi, E. Janod, and L. Cario, Optical Conductivity Measurements of $GaTa_4Se_8$ Under High Pressure: Evidence of a Bandwidth-Controlled Insulator-To-Metal Mott Transition, Phys. Rev. Lett. **110**, 037401 (2013).

[13] Y. Wang, D. Puggioni, and J. M. Rondinelli, Assessing exchange-correlation functional performance in the chalcogenide lacunar spinels GaM_4Q_8 (M = Mo, V, Nb, Ta; Q = S, Se), Phys. Rev. B **100**, 115149 (2019).

[14] M. Sieberer, S. Turnovszky, J. Redinger, and P. Mohn, Importance of cluster distortions in the tetrahedral cluster compounds GaM4 × 8 (M = Mo, V, Nb, Ta; X = S, Se): *Ab initio* investigations, Phys. Rev. B **76**, 214106 (2007).

[15] P. L. Alireza, F. Nakamura, S. K. Goh, Y. Maeno, S. Nakatsuji, Y. T. Chris Ko, M. Sutherland, S. Julian, and G. G. Lonzarich, Evidence of superconductivity on the border of quasi-2D ferromagnetism in Ca_2RuO_4 at high pressure, J. Phys.: Condens. Matter **22**, 052202 (2010).